

Excellence in Chemistry Research

Announcing our new flagship journal

- Gold Open Access
- Publishing charges waived
- Preprints welcome
- Edited by active scientists



Meet the Editors of *ChemistryEurope*



Luisa De Cola

Università degli Studi
di Milano Statale, Italy



Ive Hermans

University of
Wisconsin-Madison, USA



Ken Tanaka

Tokyo Institute of
Technology, Japan



Particle Size Effects in the Selective Hydrogenation of Alkadienes over Supported Cu Nanoparticles

Giorgio Totarella,^[a] Jan Willem de Rijk,^[a] Laurent Delannoy,^[b] and Petra E. de Jongh*^[a]

Copper is considered an excellent alternative to noble-metal selective hydrogenation catalysts. Herein, we systematically studied the effect of Cu nanoparticle size (2–10 nm) in the selective hydrogenation of 1,3-butadiene in excess of propene. The catalysts exhibited particle size-dependent activity, with particles above 4 nm being 3 to 4 times more active than the 2 nm ones, and at the same time more selective (up to 99% at almost full butadiene conversion for 7–10 nm particles). The higher activity of larger particles was ascribed to a higher

fraction of kinks and step sites, essential to activate hydrogen. The high selectivity of nanoparticulate Cu catalysts was explained by a very strong preferential adsorption of 1,3-butadiene compared to mono-olefin adsorption on the Cu surface (in particular on larger particles), as proven via adsorption measurements. These findings may guide both testing and catalyst design for reactions where hydrogen surface availability and selectivity play a key role.

Introduction

Catalysts based on earth-abundant first-row transition metals, such as Mn, Fe, Co, Ni and Cu, might play a crucial role due to ecological and economic advantages.^[1] Over the last few decades they have been proven to be highly efficient for a variety of organic transformations.^[1–3] The catalytic activity of these materials is, however, often lower than the one of noble metal counterparts, *e.g.*, Pd, Pt, Rh, Ru and Ir. For this reason, first-row transition metals are often alloyed in bimetallic formulations,^[4] promoted/doped with other elements or metal oxides, or immobilized onto activity- or stability-boosting supports.^[5] For supported metal nanoparticles, an important parameter is their particle size.^[5–8] Structure insensitive^[9–12] reactions, or better reactions for which the reaction rate scales linearly with the metal specific surface area, benefit from the presence of smaller particles for obvious reasons. For structure sensitive^[9–12] reactions, on the other hand, certain particle sizes give optimal catalytic performance and non-monotonic dependencies might appear.^[9–12]

Hydrogenation of (poly)unsaturated hydrocarbons, a well-studied model reaction for selective hydrogenation catalysts and very relevant in industrial applications,^[13–18] is considered to be a structure insensitive reaction for most substrates and most transition metal surfaces.^[10,19–21] This is well documented in particular for ethylene hydrogenation and other alkene hydrogenations that do not involve C–C cleavage.^[22] Hydrogenation of alkynes and dienes, however, presents more challenges, as multiple hydrogenated products are possible. In this case not only the activity of the catalyst has to be taken into consideration, but also its selectivity. For the hydrogenation of 1,3-butadiene, its structure sensitivity or insensitivity^[21] has not yet been reported.


Copper nanoparticles, which recently gained much attention due to their promising selectivity in relevant hydrogenation reaction, possess size-dependent hydrogenation properties in certain types of reactions.^[23–25] The effect of particle size on the activity of Cu based hydrogenation catalysts was observed for the conversion of acetone to isopropyl alcohol over differently sized Cu/SiO₂ catalysts (1.5, 14, 64, 110 and 176 nm).^[26] Particles of around 110 nm prepared via incipient wetness method were 7 times more active, in terms of turnover frequency (TOF), than similarly prepared 14 nm Cu/SiO₂ and up to 40 times more active than ion-adsorption synthesized 1.5 nm Cu/SiO₂ particles. The effect was tentatively ascribed to the electronic properties of the nanoparticles since a correlation was found between the measured TOF and the particles electrical conductivity.^[26] For particles with a size above 2–3 nm, however, electronic effects on their activity are unlikely, due to the size-insensitive local density of state of surface sites.^[27,28]


Recent work on Cu and Cu/Zn on SiO₂ catalysts^[23] indicated that the surface-dependent activity of sub-10 nm copper in methanol synthesis is due to geometric rather than electronic effects. The authors observed a three-fold increase in TOF by going from particles of 2 to 8 nm, regardless of the presence of ZnO_x as promoter.^[23] Cu/C catalysts appeared to show a similar size-dependent activity in the hydrogenation of ethyl acetate to

[a] G. Totarella, J. W. de Rijk, Prof. P. E. de Jongh
Materials Chemistry and Catalysis
Debye Institute for Nanomaterials Science
Utrecht University
3584, CG, Utrecht (The Netherlands)
E-mail: P.E.deJongh@uu.nl

[b] L. Delannoy
Sorbonne Université, CNRS, Laboratoire de Réactivité de Surface (LRS)
F-75005 Paris (France)

 Supporting information for this article is available on the WWW under <https://doi.org/10.1002/cctc.202200348>

 This publication is part of a joint Special Collection with EurJOC and EurJIC on the Netherlands Institute for Catalysis Research. Please see our homepage for more articles in the collection.

 © 2022 The Authors. ChemCatChem published by Wiley-VCH GmbH. This is an open access article under the terms of the Creative Commons Attribution License, which permits use, distribution and reproduction in any medium, provided the original work is properly cited.

ethanol;^[25] a 4-fold increase in TOF when going from 3 to 10 nm particles, with a maximum in hydrogenation activity for 6 nm particles. Regarding the 1,3-butadiene hydrogenation in presence of propene over Cu nanoparticles, recent work^[24] suggested that the hydrogenation selectivity could be size dependent as well.

In order to systematically study particle size effects, we prepared a series of supported Cu catalysts with Cu particle sizes from 2 to 10 nm and tested them for the hydrogenation of trace (3000 ppm) of 1,3-butadiene in an excess of propene. Tests at different gas flows and reactor loadings were performed to compare the catalyst selectivity at similar temperature and 1,3-butadiene conversion. Finally, 1,3-butadiene and propene adsorption/desorption experiments helped to explain the trends in selectivity.

Results and Discussion

Tuning the Cu particle size on SiO₂

A summary of the parameters used to produce the differently sized Cu nanoparticles is reported in Table 1. In particular, impregnation of the silica gel with 1 M solution of Cu(NO₃)₂ followed by either heat treatment in N₂ (350 mL min⁻¹, 2 °C min⁻¹, 2 h at 350 °C), 20% H₂/N₂ (250 mL min⁻¹, 2 °C min⁻¹, 2 h at 300 °C) or 2% NO/N₂ (350 mL min⁻¹, 2 °C min⁻¹, 2 h at 350 °C) yielded 2, 3 and 7 nm particles respectively (Table 1). Particles of around 10 nm were also obtained via thermal

decomposition under 2% NO/N₂, with the difference that the flow was applied in bottom-top configuration (fluidized bed, 350 mL min⁻¹). The Cu weight loading of these materials was 5.7 wt%. Particles of around 4 nm were obtained by impregnating the silica gel support with a 2 M solution of Cu(NO₃)₂ (10.5% final Cu wt.%) followed by direct reduction under 20% H₂/N₂ (250 mL min⁻¹, 2 °C min⁻¹, 2 h at 300 °C).

Transmission electron micrographs of selected catalysts are shown in Figure 1. Particle size distribution histograms and additional micrographs for all the catalysts can be found in the Supporting Information (Figure S1), while the relative average Cu particle size and width of the distribution can be found in Table 1. XRD measurements of the CuO crystallite sizes were in good agreement with the particles' sizes measured by TEM. CuO nanoparticles XRD profiles can be found in (Supporting) Figure S2. To conclude, we hereby show that controlling the synthesis conditions can be an excellent method to achieve good control over the CuO/Cu particle size in the range of 2 to 10 nm.

Particle size effect on catalyst activity

Figure 2 shows the evolution of the concentration of all C₄ species as function of reaction temperature for two catalysts, namely 2nm_Cu/SiO₂ and 4nm_Cu/SiO₂. Data for 3 and 7 nm have been published before,^[24] while the data for the 10nm_Cu/SiO₂ are reported in Figure S3. All the materials were pre-conditioned by exposing them to the reaction mixture for 15 h at 130 °C as described in detail elsewhere.^[24] Conversion of 1,3-

Table 1. Synthesis parameters and physicochemical properties of the silica-supported Cu catalysts.

Catalyst	Cu loading [wt%]	Gas atmosphere during thermal treatment	T _{treatment} [°C(°C/min)]	d _{TEM} ± σ _{TEM} [nm]	d _{XRD} [nm]	S _{Cu} [m _{Cu} ² g _{Cu} ⁻¹]
2nm_Cu/SiO ₂	5.7	N ₂ – 350 mL min ⁻¹ [a]	350(2)	2.0 ± 0.6	n.a	336
3nm_Cu/SiO ₂	5.7	20% H ₂ /N ₂ – 250 mL min ⁻¹ [a]	300(2)	3.5 ± 1.0	3	192
4nm_Cu/SiO ₂	10.5	20% H ₂ /N ₂ – 250 mL min ⁻¹ [a]	300(2)	4.4 ± 1.2	6	152
7nm_Cu/SiO ₂	5.7	2% NO/N ₂ – 350 mL min ⁻¹ [a]	350(2)	7.3 ± 2.4	10	92
10nm_Cu/SiO ₂	5.7	2% NO/N ₂ – 100 mL min ⁻¹ [b]	350(2)	9.9 ± 4.2	12	68

[a] Packed-bed configuration, [b] bottom-top flow (fluidized bed).

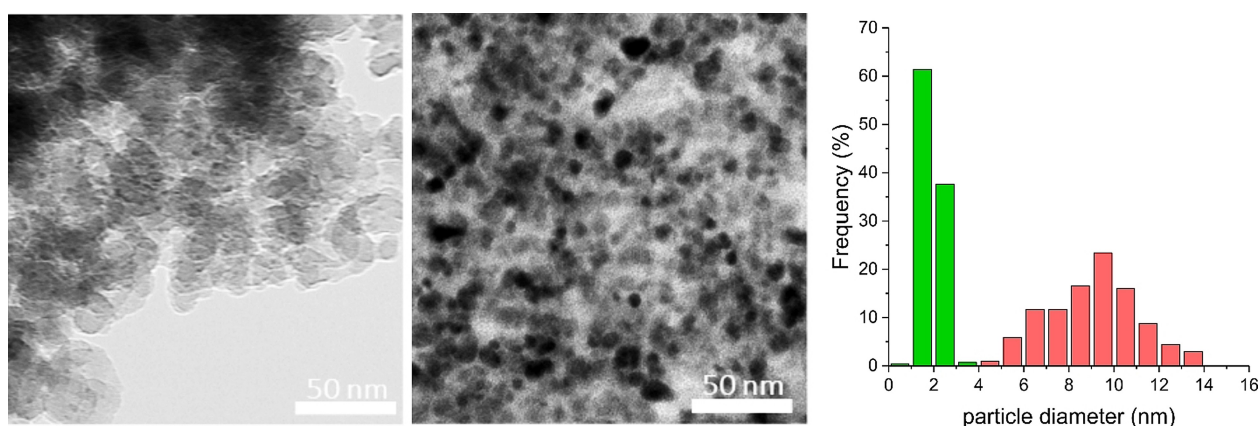


Figure 1. Transmission electron micrographs for two selected catalysts: 2nm_Cu/SiO₂ (left) and 10nm_Cu/SiO₂ (center). Particle size distribution for the two catalysts reported on the right.

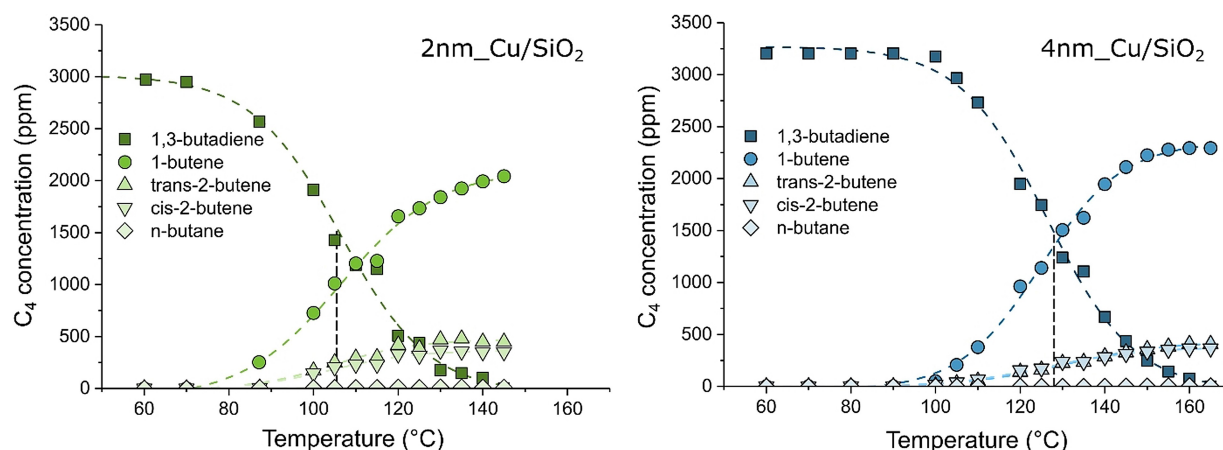


Figure 2. Concentration profiles for the reactant 1,3-butadiene and its hydrogenation products, namely 1-butene, trans-2-butene, cis-2-butene and double hydrogenated butane, as function of the reactor temperature for the catalysts 2nm_Cu/SiO₂ (left) and 4nm_Cu/SiO₂ (right). The data were collected under steady-state conditions. 1,3-butadiene/propene/H₂/He = 0.15/15/10/24.85 mL min⁻¹, 1 bar pressure, 1.28 mg Cu. GHSV: 35000 h⁻¹.

butadiene was detected at temperatures as low as 100 °C for both catalysts. The main products of hydrogenation were 1-butene (> 70%), followed by trans- and cis-2-butene (produced in similar amounts, around 10–15% at T > 120 °C). Only traces of butane were formed. Full 1,3-butadiene conversion (1,3-butadiene concentration below 50 ppm) was reached at 140 °C for the 2nm_Cu/SiO₂ catalyst and 160 °C for the 4nm_Cu/SiO₂ sample, respectively. The 1,3-butadiene concentration profiles obtained for 2 and 4 nm Cu on SiO₂ show a similar shape and slope, suggesting that both catalysts have comparable activation energies for the hydrogenation of the alkadiene. The 2 nm catalyst appears to be more active per Cu unit mass than the 4 nm catalyst. In fact, the temperature for which 50% conversion of 1,3-butadiene is reached is 106 °C and 126 °C respectively for 2 and 4 nm particles.

To better assess the differences in activity, the experiments were repeated at similar conversions and in the same temperature range (100–170 °C) by adjusting the amount of catalyst loaded in the reactor. An example of 1,3-butadiene conversion vs. temperature data collected for 2 and 4 nm Cu is plotted in Figure 3A (see Supporting Figure S4 for all catalysts), while the turnover frequencies (TOF) calculated for the different particle sizes are depicted in Figure 3B. As it can be observed from the data reported in Figure 3A, the catalysts show almost the same 1,3-butadiene conversion when tested at copper loadings corresponding to 0.417 m_{Cu}² for 2nm_Cu/SiO₂ (45% conversion) and 0.099 m_{Cu}² for 4nm_Cu/SiO₂ (50% conversion). This suggests that the 4 nm particles are around 4 times more active than 2 nm ones per unit Cu surface area. This difference is also reflected in the turnover frequencies (mmol of H₂ consumed per hour per mmol of Cu present at the nanoparticle surface, see *Experimental Section: Structural Characterization*) as calculated at 130 °C for all catalysts. As expected, the TOF of Cu nanoparticles increases 4-fold by going from 2 to 4 nm Cu (24 h⁻¹ vs. 107 h⁻¹, Figure 3B). Interestingly, there is only a limited change in activity for particles above 4 nm (7 and 10 nm Cu were > 3 times more active than 2 nm particles). To assess the origin of the difference in activity between particles,

the conversion data were modelled in terms of Arrhenius plots, depicted in Figure 3C. The kinetic model applied for the study of the 1,3-butadiene conversion data is based on previous work,^[24] while the packed bed reactor design equation (integral form) used for extrapolating the kinetic constant is reported in Supporting Information Section 2. The reaction rates were normalized to the Cu surface area instead of catalyst weight (Cu surface areas are reported in Table 1 as S_{Cu} , calculations can be found in ref.^[24]). The activation energy for the hydrogenation of 1,3-butadiene was independent of the Cu particle size (Figure 3D). In particular, a value of E_{act} equal to 62 ± 3 kJ mol⁻¹ was found, well in line with previously reported data for the hydrogenation of 1,3-butadiene from alkene-free streams on model systems.^[32] The difference in catalyst activity is hence due to the different pre-exponential A values (reported in Table 2 as A_{bd}). The 4 nm Cu on SiO₂, the most active catalyst as normalized per Cu area, showed ~4 times higher pre-exponential factor, hence activity, than the smallest Cu nanoparticles investigated.

The same activation energy for the different Cu particle sizes suggests that the nature of the active site involved in the determining step for the hydrogenation of 1,3-butadiene to butenes is the same in all catalysts. This indicates that size-dependency of the activity, especially in the range 2–4 nm, is probably linked to structural/geometric effects than electronic ones. The observation is in line with the reported size-insensitivity of electron-acceptor/donor behavior of Cu particles above 1–2 nm in size.^[5,23,25,27,28] By assuming the same reaction pathway for the hydrogenation of 1,3-butadiene on all the differently sized Cu nanoparticles, the numerical value of the pre-exponential factor (Table 2) can hence be used as an indirect measure of the relative abundance of active sites, or “active site – reactant” adducts. Furthermore, the 1,3-butadiene reaction rate order is first-order in hydrogen pressure, zeroth-order in propene pressure and fractional (0.25) order in 1,3-butadiene partial pressure (see Supporting Information Section 2).^[24] The reaction rate is hence limited by the availability of activated hydrogen on the surface of the Cu

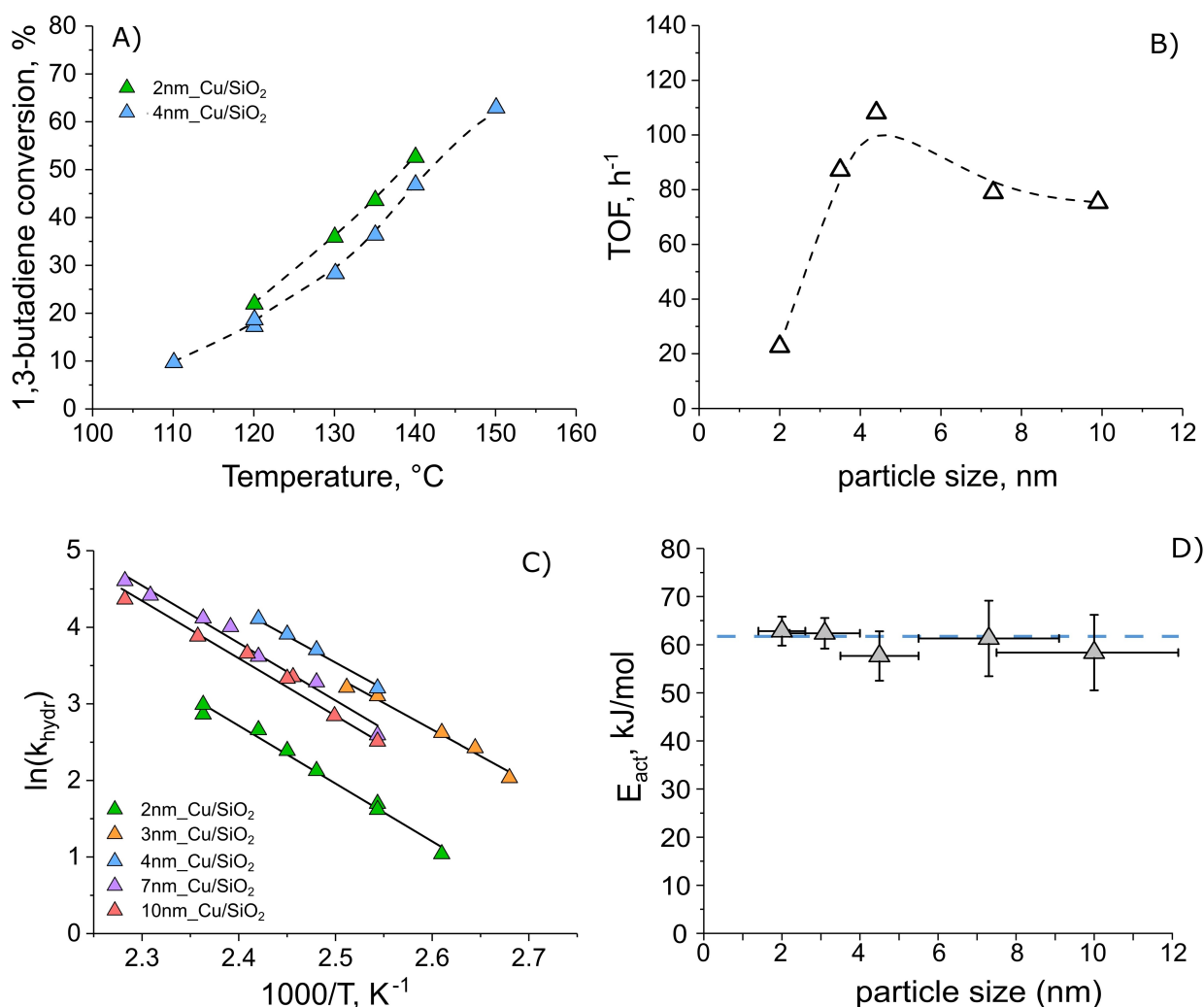


Figure 3. A) 1,3-butadiene conversion experiments carried out at similar conversion level for 2 and 4 nm particles. In both cases, the 1,3-butadiene molar flow rate to the reactor was kept the same ($0.552 \text{ mmol h}^{-1}$ 1,3-butadiene; concentration of all gases as in Figure 2), while the amount of catalyst loaded was adjusted in order to have 0.417 and 0.099 m^2 of exposed Cu for 2 and 4 nm particles, respectively); B) turnover frequency (TOF) calculated at 130°C from total hydrogen consumption for all the different particle sizes investigated; C) Arrhenius plot and D) activation energy vs. Cu particle size for the 2, 3, 4, 7 and 10 nm Cu on SiO_2 catalysts as calculated from 1,3-butadiene consumption rate (conversion data reported in Supporting Figure S4). Average E_{act} shown in Figure 3D with a dashed line is equal to 62 kJ mol^{-1} . Pre-exponential factor (A_{bd}) values were obtained by using a fixed value for the activation energy (62 kJ mol^{-1}). A comparison of TEM for fresh and used catalyst for 2 nm Cu, the catalyst with the smallest particles and hence expected to be most prone to particle growth, can be found in Supporting Figure S5.

Table 2. Pre-exponential factor for the 1,3-butadiene hydrogenation to butenes (A_{bd}), propene hydrogenation in absence of 1,3-butadiene (A_{p}), propene hydrogenation in presence of 1,3-butadiene (A_{pwbd}) and the ratio between A_{p} and A_{pwbd} .

Sample name	A_{bd} [$\text{mols}^{-1} \text{ m}^{-2} \text{ bar}^{-1.25}$]	A_{p} [$\text{mols}^{-1} \text{ m}^{-2}$]	A_{pwbd} [$\text{mols}^{-1} \text{ m}^{-2}$]	Ratio $A_{\text{p}}/A_{\text{pwbd}}$
2nm_Cu/SiO ₂	271	0.093	0.011	8
3nm_Cu/SiO ₂	1168	0.055	0.007	9
4nm_Cu/SiO ₂	1320	0.010	0.001	12
7nm_Cu/SiO ₂	809	0.033	n.a. ^[a]	n.a. ^[a]
10nm_Cu/SiO ₂	704	0.180	0.0003	700

[a] propane concentration too low for performing Arrhenius plot fitting.

nanoparticles. This is in agreement with literature evidence of low deuterium-hydrogen exchange for Cu catalysts under typical hydrogenation conditions, pointing out to low concentration of activated hydrogen on the Cu surface.^[33,34]

An analogous effect of the nanoparticle size on Cu activity, with a maximum at diameters above 4–6 nm, was observed for other gas phase hydrogenation reactions. In the case of methanol synthesis, van der Berg et al.,^[23,35] for instance,

observed an increase in TOF by a factor of 3 going from 2 to 8 nm copper particles for both Cu and promoted Cu (CuZn) supported nanoparticles. Structural effects on the hydrogenation activity of Cu nanoparticles were observed also in case of the hydrogenation of ethyl acetate to ethanol for C- supported Cu.^[25] In this case, a maximum activity was observed at 6 nm, which stayed rather constant up to 13 nm Cu. In both cases the authors ascribed the observed effect to the reaction taking place at surface sites with a unique configuration of several copper atoms such as step-edge and kink sites, identified as responsible for H₂ activation. This observation that not all Cu atoms on the surface of NPs have the same reactivity (in the size range below 10 nm) has also been reported in recent literature.^[35] The activity trends described in this work, as well as in ref.^[23,25] correlate with the theoretical fraction of Cu step (B5A, B5B on fcc metals) and kink (B6) surface sites, usually found at the interface of Cu(111) and Cu(100) (the geometrical equivalent of high Miller index Cu(311), Cu(221), Cu(321) planes). The maximum relative abundance of these sites it's interestingly expected at around 4–6 nm.^[23,25,36–38]

In conclusion, it can thus be proposed that the 1,3-butadiene hydrogenation activity described in this work is strongly dependent on the abundance of step and kink sites over the Cu surface. These in turn control the surface availability/concentration of hydrogen and henceforth the reaction rate. This activity pattern seems to be in common with other Cu-catalyzed gas phase hydrogenations.

Particle size effects on catalyst selectivity

The selectivity of the catalysts was evaluated in terms of butenes produced (1-butene + trans-2-butene + cis-2-butene) vs. both the consumption of 1,3-butadiene (Figure 4A) and the total amount of hydrogen consumed by the catalyst^[24] (equivalently, this selectivity is defined as the ratio of the production rate of butenes to the sum of consumption rates of 1,3-butadiene to butenes plus consumption rate of butenes and propene, Figure 4B). The first captures the ability of the catalyst to hydrogenate 1,3-butadiene to butenes without further over hydrogenation to butane. The second reflects the ability of the catalyst to hydrogenate 1,3-butadiene against any other alkene in the stream (i.e.: propene), which helps unravelling alkadiene-alkene hydrogenation competition as well as being a critical parameter in practical applications.^[13–18,24] As the concentration of propene in the reaction mixture is very high (30%, versus 0.3% 1,3-butadiene), conversion of a small fraction of the propene can drastically lower the total selectivity of the catalyst (e.g.: 100% 1,3-butadiene conversion and 1% of propene conversion corresponds to a catalyst selectivity of 50%). Lastly, Figure 4C displays the total selectivity to butenes as function of the Cu particle size.

The catalyst that displayed the lowest 1,3-butadiene to butenes selectivity in the entire series was 2nm_Cu/SiO₂. The selectivity for this catalyst, however, was still rather high due to very limited formation of n-butane (diene to butene selectivity above 99%, Figure 4A). Catalysts with larger particle size displayed formation of similar amounts of n-butane, usually well below

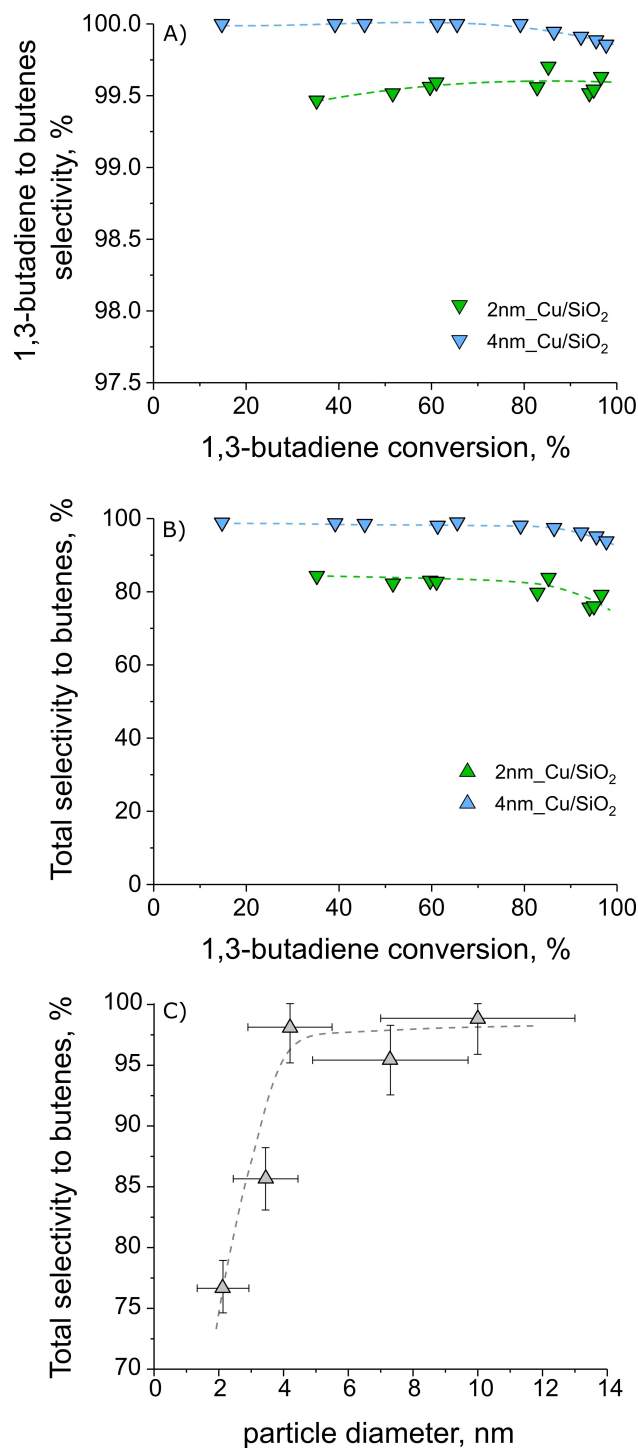


Figure 4. A) 1,3-butadiene to butenes selectivity (ratio between production rate of butenes to consumption rate of 1,3-butadiene) as function of 1,3-butadiene conversion for the reduced 2 and 4 nm Cu; B) total selectivity to butenes (defined as the ratio of the production rate of butene to the sum of the consumption rates of 1,3-butadiene, butenes and propene) as a function of 1,3-butadiene conversion for the reduced 2 and 4 nm Cu. Pre-treatment, reaction conditions and testing methodology as in Figure 2; C) Selectivity to butenes at 130 °C as a function of the particle size for 5–20% of 1,3-butadiene conversion (dashed lines: guide for the eye).

50 ppm (see Figure S3), and hence a 1,3-butadiene to butene selectivity >99.5% in the entire 1,3-butadiene conversion range investigated (e.g.: see Figure 4A for 4nm_Cu/SiO₂). In terms of *n*-butane formed, the catalysts displayed similar behavior within measurement error. What really differentiated the different samples was the amount of propene consumed, which varied drastically between the different particle sizes, thus affecting the total selectivity of the catalyst (e.g.: the concentration of propene at 50% 1,3-butadiene conversion was 10 and 305 ppm for 4 and 2 nm particles, respectively; see Supporting Figure S6). For this reason, the rest of the discussion will focus on the total catalyst selectivity, referred to as “selectivity to butenes” from this point of the text onwards. The selectivity to butenes was above 70% for all the catalysts investigated, with the 4nm_Cu/SiO₂ exhibiting the highest selectivity (Figure 4B). A minor selectivity decrease was found at high diene conversions for 4 nm Cu (from 98.8% to 93.8% selectivity by going from 65 to 98% 1,3-butadiene conversion). For the 2nm_Cu/SiO₂, the selectivity also slightly decreases with increasing the 1,3-butadiene conversion, from 85% at 35% conversion to 78% at 98% 1,3-butadiene conversion.

Direct comparison of selectivities is not trivial since the selectivity depends both on the temperature and on the concentration of all the species in the reactor bed during catalysis.^[24,39] For this reason, tests at the same temperature (130 °C) and similar 1,3-butadiene conversion (5–20%; data at ~80% conversion are reported in Figure S7) were carried out. The data reveal a clear trend in selectivity, with the 2 nm particles being the least selective ones (77%) of the entire set. Interestingly, the selectivity to butenes increases by going from 2 to 4 nm (77, 86 and 98%, respectively for 2, 3 and 4 nm) and levels off to more than 95% for 4, 7 and 10 nm particles. This shows that the larger Cu nanoparticles (equal or above 4 nm) are the most selective ones.

Separate propene hydrogenation experiments were carried out to clarify the origin of the high catalyst selectivity. The first test was carried out with additional 1,3-butadiene in the reactor feed, the second experiment in its absence. An example of these data can be found in Figure 5A for the sample 2nm_Cu/SiO₂. Data are also reported as natural logarithm of the reaction rate of the propene hydrogenation reaction against the reciprocal temperature (frame 5B), assuming zero order reaction kinetic in propene and hydrogen (hence the reaction rate is equal to the kinetic constant of the reaction, $k_{\text{prop.hydr}}$). This assumption is justified considering differential conversion conditions, due to rather constant concentrations for propene and hydrogen along the reactor bed. The addition of 1,3-butadiene to the reaction mixture causes a sharp decrease in propane production (almost 10-fold decrease at 150 °C). The drastic decrease of the propene hydrogenation rate by the presence of 1,3-butadiene was observed for all the catalyst of the series.

Strikingly, the slope of the Arrhenius curves obtained for the propene-only case (corresponding to $E_{\text{act}} = 38$ kJ/mol) is independent of the presence of 1,3-butadiene (see Figure 5B and Figure S8). Furthermore, the apparent activation energy for propene hydrogenation is lower than for 1,3-butadiene (38 vs 62 kJ/mol, respectively), but nevertheless propene hydrogenation activity of the sample(s) is strongly hindered by the presence of 1,3-butadiene. The change in reaction rate is hence explained by a change in pre-exponential factor. The ratio between the pre-exponential factors obtained in the case of hydrogenation of propene carried out without and with 3000 ppm of 1,3-butadiene in the reaction mixture was calculated for all the catalysts (Table 2). This ratio increases along with the particle size (8, 9 and 12 and 700 for 2, 3, 4 and 10 nm Cu on SiO₂).

Lastly, hydrocarbon adsorption experiments were carried out on two selected catalysts (3nm_Cu/SiO₂, 7nm_Cu/SiO₂) to verify whether the impact of the presence of 1,3-butadiene on

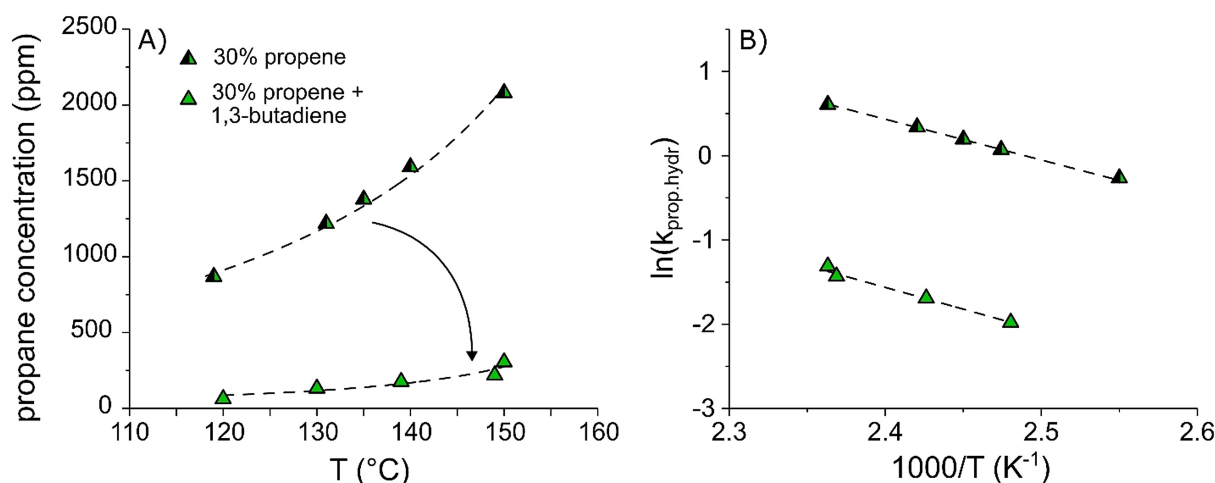


Figure 5. A) Propane concentration vs. temperature during the hydrogenation of 30% propene in He in presence (green half triangles) and absence (green full triangles) of 0.3% of 1,3-butadiene for the sample 2nm_Cu/SiO₂; B) corresponding Arrhenius plot showing the natural logarithm of the propene hydrogenation kinetic constant. Conditions: 1,3-butadiene/propene/H₂/He = 0.15:(or 0):15:10:24.85:(or 25.00), 1 bar, 5.6 mg Cu. GHSV: 52500 h⁻¹. Due to the low propene conversion (below 1%) the reaction rate was assumed to be zeroth order in propene partial pressure and zeroth order in hydrogen partial pressure.

the propene hydrogenation can be explained by the stronger adsorption energy for 1,3-butadiene compared to propene. During these experiments, pre-reduced catalysts were exposed to either 1,3-butadiene or a mixture of 1,3-butadiene and propene in He (0,6% concentration for each hydrocarbon, 25 mL min⁻¹ total; the conditions were adjusted to have proper time-resolution and hence quantifiable hydrocarbon uptake). The diluent, in this case, acts both as a carrier and tracer. The delay between the He signal and any of the two hydrocarbons is proportional to the amount of alkadiene or alkene adsorbed. The results, also known as breakthrough curves, are reported in Figure 6 in terms of relative amount of 1,3-butadiene and/or propene at the inlet of the reactor (a value of 100% means that the concentration of the specific molecule in the inlet and the outlet of the reactor is exactly the same).

Reference experiments carried out on pre-dried silica gel only shown simultaneous emission of He and hydrocarbons from the exposed packed bed, hence no hydrocarbon uptake by the support itself. For both the 3 and 7 nm supported Cu nanoparticles, a clear delay in the signal of the hydrocarbons was observed (see Figure 6), confirming the uptake of hydrocarbons Cu nanoparticles. Release of 1,3-butadiene upon heating was verified via DSC experiment for the 7nm Cu/SiO₂,

see Supporting Figure S9. In the 1,3-butadiene/He experiments, the amount of 1,3-butadiene adsorbed was equal to 0.014 and 0.018 mmol m_{Cu}⁻² respectively for 3 nm and 7 nm Cu. Upon addition of propene to the mixture, a modest, yet significant amount of propene was adsorbed by both materials (around 0.001 mmol m_{Cu}⁻² for 3 and 7 nm Cu). Interestingly, both materials were able to retain 1,3-butadiene even in presence of propene, with limited to no change in the uptake amount of the diene (unaltered for the 7 nm Cu/SiO₂; from 0.014 mmol m_{Cu}⁻² to 0.008 mmol m_{Cu}⁻² for 3 nm Cu/SiO₂). This suggests that the adsorption of 1,3-butadiene was stronger than for propene, in particular for the larger particles. This difference in relative adsorption strength can potentially explain the difference in selectivity between smaller particles (2 and 3 nm) and the more selective larger ones (4 nm and above).

The hydrogenation of 1,3-butadiene and propene displayed different activation energies (62 vs. 38 kJ mol⁻¹, respectively), suggesting that the energy barrier of the hydrogenation reaction (activation energy) is more likely to be the insertion of activated hydrogen on the hydrocarbon substrate rather than hydrogen dissociation. This reinforces the hypothesis that the reaction selectivity depends on the relative concentration of the two hydrocarbons presence on the surface, with the reaction kinetic

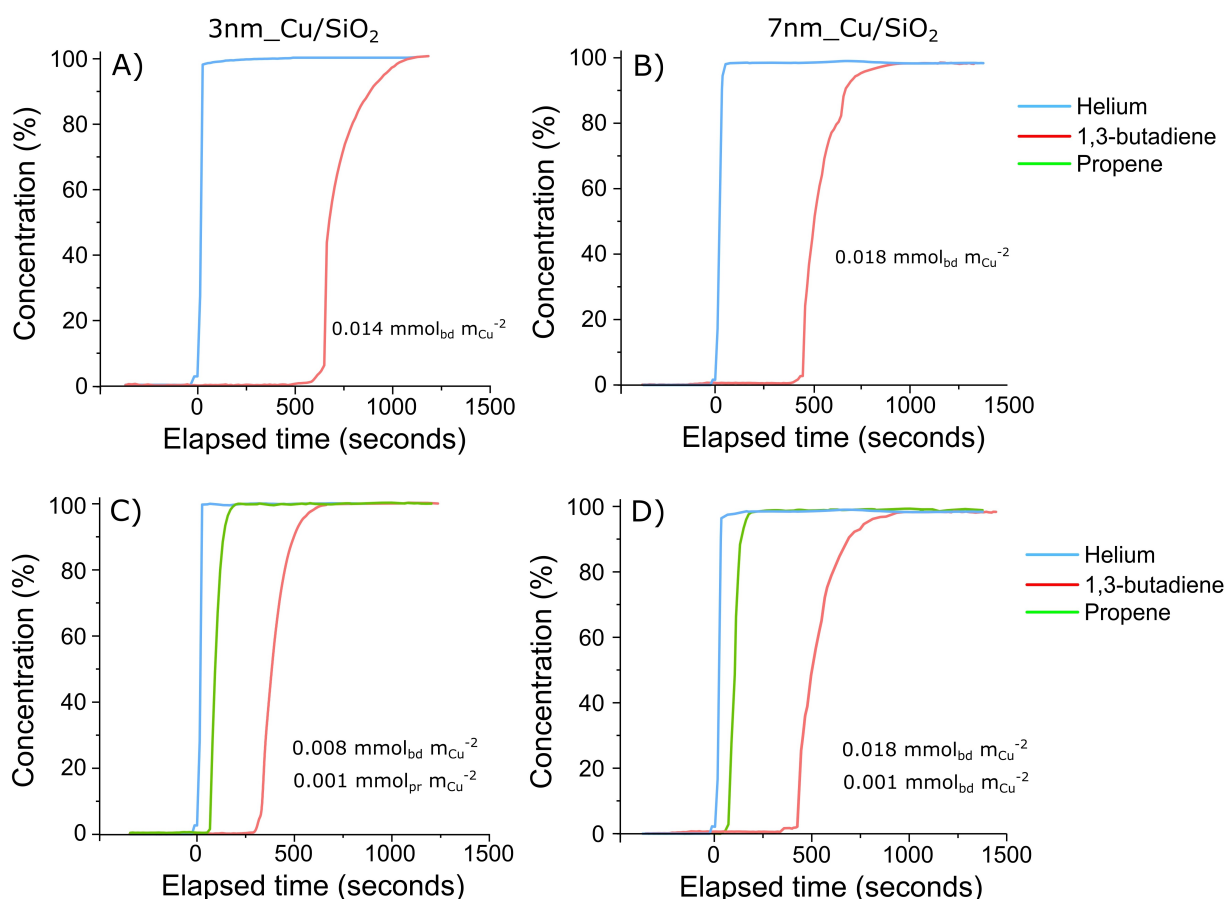


Figure 6. Hydrocarbon adsorption experiments for 3nm_Cu/SiO₂ and 7nm_Cu/SiO₂ catalyst. The pre-reduced catalysts (see Methods) were exposed to either i) 0.6% 1,3-butadiene in He (Figure 6A: 3nm_Cu/SiO₂, Figure 6B: 7nm_Cu/SiO₂) or ii) 0.6% 1,3-butadiene + 0.6% propene in He (the 0.6% propene concentration was adjusted in order to increase the time resolution of the experiment; Figure 6C: 3nm_Cu/SiO₂, Figure 6D: 7nm_Cu/SiO₂). Helium is used both as diluent and inert tracer. Amount of catalyst loaded = 0.9 g. Gas flow: 25 mL min⁻¹. Temperature = 30 °C.

following a Langmuir-Hinshelwood type of mechanism.^[24,40,41] For particles above 2 nm, electronic effects are unlikely. Moreover, electronic effects would be expected to also change the selectivity, as an increase in electron-acceptor character would promote $\pi\sigma$ coordination of the semi-hydrogenated butenyl intermediate (π -butenyl), leading to formation of trans-2-butene at the expenses of 1-butene.^[24,32,42] A rather similar selectivity to 1-butene observed for all samples (Figure S3), as well as size insensitive activation energies for the hydrogenation of 1,3-butadiene and propene. This strongly suggests that electronic effects cannot explain the dependence of selectivity on particle size. In this work, the lowest selectivity was observed for 2 and 3 nm particles. The surface of these small particles (~2 nm) is known to be richer in corner and edge sites.^[25,36] Their high abundancy can hence lead to a higher coverage and activation of smaller molecules (or smaller semi-hydrogenated intermediates), as in this case propene, lowering the selectivity of the catalyst towards hydrogenation of 1,3-butadiene. In conclusion, while the hydrogen surface concentration dictates the catalyst activity, the difference between the adsorption of the hydrocarbons (butadiene and propene) on the exposed Cu-nanoparticles is responsible for the catalyst selectivity. The ideal Cu catalyst has a surface consisting of a large fraction of steps and kinks sites (high activity) and is poor in corner and edge sites (linked to low selectivity). Optimal activity and almost full selectivity to butenes are thus achieved on Cu particles above 4 nm.

Conclusions

Differently sized copper nanoparticles (from 2 to 10 nm) catalysts were synthesized and used for the selective hydrogenation of 1,3-butadiene to butenes in presence of a large excess of propene. The 1,3-butadiene hydrogenation activity of nanoparticulate Cu increased with increasing Cu particle size up to 4 nm (4-fold increase in pre-exponential factor from 2 to 4 nm particles). In addition, the 1,3-butadiene reaction rate appeared to be limited by availability of H on the surface of Cu, with an associated activation energy equal for all five catalysts. The increase in activity with increasing particle size was ascribed to the increase in relative abundance of hydrogenation active sites, in particular steps and kinks, by moving from 2 to 4–10 nm. Kinetic analysis of the hydrogenation of 1,3-butadiene and propene, together with hydrocarbon adsorption experiments, proved that the selectivity of nanoparticulate Cu is governed by the preferential adsorption on the Cu surface of alkenes rather than alkenes. This preferential hydrocarbon uptake is favored by a low surface concentration of corner and edge sites. Lastly, near full selectivity (~99%) to butenes was observed for 7–10 Cu nm particles.

Experimental Section

Details on the chemicals used for the synthesis and gas feeds are reported in the Supporting Information (Section 1).

Synthesis of Cu/SiO₂. Cu nanoparticles on silica were synthesized via incipient wetness impregnation and drying following a method reported elsewhere for silica SiO₂ gel supports.^[24,29,30] The impregnation solution concentration and the thermal treatment conditions were tweaked to obtain particles of 2, 3, 4, 7 and 10 nm (final Cu weight loading equal to 5.7 wt%, except for 4 nm Cu, for which the weight loading was equal to 10.5 wt%). After synthesis, all samples were left to cool to room temperature, purged with 20 vol% O₂/N₂ flow (100 mL min⁻¹ g⁻¹) and heated up to 250 °C in the same gas mixture (heating ramp of 2 °C min⁻¹, isothermal hold of 2 h, 100 mL min⁻¹ gas flow for each gram of dry material). The samples (supported CuO nanoparticles) were exposed to air and stored in closed vials at room temperature.

Structural characterization. XRD analysis was carried out with a Bruker D2 Phaser with a Co K α (1.78897 Å) radiation source. The diffractograms were recorded in the 2 θ range of 15 to 90° with a step size of 0.05°. Analysis of the diffractograms was carried out with DIFFRAC-SUITE TOPAS software. Transmission electron micrographs of the Cu/SiO₂ catalysts were obtained on a Thermo Fisher Talos L120 C apparatus, operated at 120 kV. Prior to TEM imaging, the silica-supported samples were ultramicrotomed in order to increase the contrast between the amorphous silica gel support and the Cu nanoparticles. The catalyst grains (< 75 μ m) were embedded in a two-component epoxy resin (Epoxy, EMS) and cured at 60 °C for 24 h. The embedded catalysts were sliced into 50 nm nominal thickness sections by means of a Diatome Ultra 35° diamond knife mounted on a Reichert-Jung Ultracut E microtome machine. The slices were deposited on a TEM grid and analyzed. Average particle sizes were defined as $d_{TEM} = \sum_i (d_{NP,i}^3 / d_{NP,i}^2)$, while the width of the distribution was taken as the standard deviation. The number of surface copper atoms was calculated using a copper density of 1.46×10^{19} atoms per square meter of exposed Cu surface area. The latter was calculated by assuming a spherical particle shape and using the equation $S_{Cu} = 6000 / d_{TEM} \rho_{Cu}$ where S_{Cu} is the specific copper surface area ($m^2_{Cu} g_{Cu}^{-1}$), d_{TEM} is the mean particle diameter and ρ_{Cu} is the copper density (8.92 g cm⁻³).^[30] The Cu particle sizes (after reduction of the pre-catalyst prior to catalytic tests) were assumed to be the same as the CuO particle size in XRD and TEM analysis.

Catalytic tests. Catalytic tests were performed using a tailor-made gas-phase hydrogenation set-up previously described by Masoud et al.^[31] The experiments were carried out by loading a mixture of each individual sample (sieve fraction 75–150 μ m; total amount of copper loaded in the reactor 1.28 mg unless otherwise specified), and 150 mg SiC as thermal diluent (sieve fraction 212–425 μ m) in a U-shaped Pyrex packed bed microreactor (internal diameter 4 mm). Prior to the test, the catalysts were reduced in situ under pure H₂ flow (50 mL min⁻¹) from RT to 250 °C (ramp 2 °C min⁻¹) and kept at 250 °C for 90 min. Hereafter, the catalysts were put into contact with the reaction mixture (0.3% butadiene, 30% propene, 20% hydrogen, and helium for balance with a flow rate of 50 N mL min⁻¹, 1 bar). Tests were conducted at temperatures between 100 and 200 °C. The concentrations of the products and unconverted reactants was monitored every 15 minutes via gas chromatography using a Flame Ionization Detector (GC-FID, hydrocarbons detected: C1–C4). The composition of the gas mixture fed into the reactor was monitored at the beginning and at the end of each catalytic run by by-passing the reactor bed.

Hydrocarbons adsorption/desorption tests. Propene and 1,3-butadiene adsorption tests were carried out by adapting the set-up used for the catalytic tests. In particular, the GC sampling line was connected to a fast mass spectrometer apparatus (Hiden Analytical QGA) and the reactor (4 mm ID) was replaced with a larger (12 mm ID) in order to accommodate a larger amount of catalyst. Prior to the measurement, 900 mg of pristine catalyst was loaded into an 8 mm ID reactor and pre-reduced in situ under pure H₂ flow

(50 mL min⁻¹) from RT to 250 °C (ramp 2 °C min⁻¹) and kept at 250 °C for 90 min. The gas atmosphere was then switched to pure N₂ (50 mL min⁻¹) for 5 minutes at 250 °C and then the reactor was rapidly cooled down in the same N₂ atmosphere to 30 °C. After 15 minutes of temperature stabilization and gas mixture background measurement, the gas atmosphere was switched to either 0.3% 1,3-butadiene in He (25 mL min⁻¹ total) or 0.6% propene + 0.3% 1,3-butadiene in He (25 mL min⁻¹ total; gas mixture concentrations were chosen in order to have a reliable control on the gas flow and optimal temporal resolution). Data were collected every 15 seconds until steady state concentrations of the gas at the inlet of the reactor were reached. For one selected sample (7 nm Cu particles on SiO₂), a DSC measurement was carried out after saturation in 0.3% 1,3-butadiene in He (25 mL min⁻¹ total, See Supporting Information). The measurement was done in air-free environment under Ar flow (heating/cooling ramp of 10 °C min⁻¹).

Author information

Corresponding Author: Petra E. de Jongh (email: P.E.deJongh@uu.nl), David de Wiedgebouw, Universiteitsweg 99, 3584 CG Utrecht.

Author Contributions: G.T., P.E.d.J., J.vdR. and L.D. designed the catalytic experiments. G.T. and J.vdR designed the adsorption experiments. G.T. synthesized and characterized the SiO₂ CuO nanoparticles. G.T. carried out the catalytic experiments and analyzed the data. G.T. and P.E.d.J. wrote the paper. P.E.d.J. conceived and supervised the project. All authors discussed the results and edited the manuscript.

Acknowledgment

The authors gratefully acknowledge NWO (NWO Vici 16.130.344) for overall funding and support.

Conflict of Interest

The authors declare no conflict of interest.

Data Availability Statement

The data that support the findings of this study are available from the corresponding author upon reasonable request.

Keywords: copper · heterogeneous catalysts · selective hydrogenation · supported nanoparticles · particle size effects

- [1] R. Gebbink, M. Moret, *Non-Noble Metal Catalysis: Molecular Approaches and Reactions*, Wiley, 2019.
- [2] M. B. Gawande, A. Goswami, F. X. Felpin, T. Asefa, X. Huang, R. Silva, X. Zou, R. Zboril, R. S. Varma, *Chem. Rev.* **2016**, *116*, 3722–3811.
- [3] D. Wang, D. Astruc, *Chem. Soc. Rev.* **2017**, *46*, 816–854.
- [4] R. Ferrando, J. Jellinek, R. L. Johnston, *Chem. Rev.* **2008**, *108*, 846–904.

- [5] B. R. Cuenya, *Thin Solid Films* **2010**, *518*, 3127–3150.
- [6] D. Astruc, F. Lu, J. R. Aranzas, *Angew. Chem. Int. Ed.* **2005**, *44*, 7852–7872; *Angew. Chem.* **2005**, *117*, 8062–8083.
- [7] A. T. Bell, *Science* **2003**, *299*, 1688–1691.
- [8] L. Liu, A. Corma, *Chem. Rev.* **2018**, *118*, 4981–5079.
- [9] N. Musselwhite, G. A. Somorjai, *Top. Catal.* **2013**, *56*, 1277–1283.
- [10] G. A. Somorjai, *Catal. Lett.* **1991**, *7*, 169–182.
- [11] M. B. Taghavi, G. M. Pajonk, S. J. Teichner, *J. Colloid Interface Sci.* **1979**, *71*, 451–465.
- [12] M. Boudart, in *Adv. Catal.*, Academic Press, **1969**, pp. 153–166.
- [13] L. Delannoy, G. Thrimurthulu, P. S. Reddy, C. Méthivier, J. Nelayah, B. M. Reddy, C. Ricolleau, C. Louis, *Phys. Chem. Chem. Phys.* **2014**, *16*, 26514–26527.
- [14] R. P. Arganbright, *Selective Hydrogenation of Dienes and Acetylenes in C₃ Streams*, **1994**, WO 94/04477.
- [15] F. Studt, F. Abild-Pedersen, T. Bligaard, R. Z. Sørensen, C. H. Christensen, J. K. Nørskov, *Science* **2008**, *320*, 1320–1322.
- [16] Z. Wang, G. Wang, C. Louis, L. Delannoy, *Res. Chem. Intermed.* **2021**, *47*, 91–116.
- [17] K. K. Pant, S. K. Gupta, E. Ahmad, *Catalysis for Clean Energy and Environmental Sustainability*, Springer International Publishing, **2021**.
- [18] B. Bridier, N. López, J. Pérez-Ramírez, *Dalton Trans.* **2010**, *39*, 8412–8419.
- [19] S. D. Jackson, G. D. McLellan, G. Webb, L. Conyers, M. B. T. Keegan, S. Mather, S. Simpson, P. B. Wells, D. A. Whan, R. Whyman, *J. Catal.* **1996**, *162*, 10–19.
- [20] P. S. Cremer, G. A. Somorjai, *J. Chem. Soc. Faraday Trans.* **1995**, *91*, 3671–3677.
- [21] J. P. Boitiaux, J. Cosyns, E. Robert, *Appl. Catal.* **1987**, *32*, 145–168.
- [22] J.-W. Yang, W.-T. Zheng, Z. Hu, M. Zhang, B.-Q. Xu, *ACS Catal.* **2018**, *8*, 10254–10260.
- [23] R. van den Berg, G. Prieto, G. Korpershoek, L. I. van der Wal, A. J. van Bunningen, S. Lægsgaard-Jørgensen, P. E. de Jongh, K. P. de Jong, *Nat. Commun.* **2016**, *7*, 1–7.
- [24] G. Totarella, R. Beerthuis, N. Masoud, C. Louis, L. Delannoy, P. E. de Jongh, *J. Phys. Chem. C* **2021**, *125*, 366–375.
- [25] R. Beerthuis, J. W. de Rijk, J. M. S. Deeley, G. J. Sunley, K. P. de Jong, P. E. de Jongh, *J. Catal.* **2020**, *388*, 30–37.
- [26] R. S. Rao, A. B. Walters, M. A. Vannice, *J. Phys. Chem. B* **2005**, *109*, 2086–2092.
- [27] R. A. Van Santen, *Acc. Chem. Res.* **2009**, *42*, 57–66.
- [28] A. S. Crampton, M. D. Rötzer, C. J. Ridge, F. F. Schweinberger, U. Heiz, B. Yoon, U. Landman, *Nat. Commun.* **2016**, *7*, 1–12.
- [29] G. Wang, R. van den Berg, C. de Mello Donega, K. P. de Jong, P. E. de Jongh, *Appl. Catal. B* **2016**, *192*, 199–207.
- [30] P. Munnik, M. Wolters, A. Gabrielsson, S. D. Pollington, G. Headdock, J. H. Bitter, P. E. de Jongh, K. P. de Jong, *J. Phys. Chem. C* **2011**, *115*, 14698–14706.
- [31] N. Masoud, L. Delannoy, C. Calers, J. J. Gallet, F. Bournel, K. P. de Jong, C. Louis, P. E. de Jongh, *ChemCatChem* **2017**, *9*, 2418–2425.
- [32] G. C. Bond, *Metal-Catalysed Reactions of Hydrocarbons*, Springer US, **2005**.
- [33] J. J. Phillipson, P. B. Wells, G. R. Wilson, *J. Chem. Soc. A* **1969**, 1351–1363.
- [34] A. J. Bates, Z. K. Leszczynski, J. J. Phillipson, P. B. Wells, G. R. Wilson, *J. Chem. Soc. A* **1970**, 2435–2441.
- [35] W. Hengwei, J. Lu, *Chin. J. Chem.* **2020**, *38*, 1422–1444.
- [36] P. van Helden, I. M. Giobici, R. L. J. Coetzer, *Catal. Today* **2016**, *261*, 48–59.
- [37] R. Van Hardeveld, F. Hartog, *Surf. Sci.* **1969**, *15*, 189–230.
- [38] T. L. Einstein, in *Handb. Cryst. Growth*, Elsevier, **2015**, pp. 215–264.
- [39] A. Hugon, L. Delannoy, C. Louis, *Gold Bull.* **2009**, *42*, 310–320.
- [40] D. Seth, A. Sarkar, F. T. T. Ng, G. L. Rempel, *Chem. Eng. Sci.* **2007**, *62*, 4544–4557.
- [41] K. J. Laidler, R. E. Townshend, *Trans. Faraday Soc.* **1961**, *57*, 1590–1602.
- [42] R. B. Moyes, P. B. Wells, J. Grant, N. Y. Salman, *Appl. Catal. A* **2002**, *229*, 251–259.

Manuscript received: March 10, 2022
Revised manuscript received: June 19, 2022
Accepted manuscript online: July 13, 2022
Version of record online: August 9, 2022